Anisotropic thermal expansion in LiCaAlF$_6$ and LiSrAlF$_6$

Andrzej Grzechnik[1,5]**, Vladimir Dmitriev**[2]**, Hans-Peter Weber**[2,3]**, Jean-Yves Gesland**[4] **and Karen Friese**[1]

[1] Departamento de Física de la Materia Condensada, Universidad del País Vasco, Apartado 644, Bilbao, E-48080, Spain
[2] Group 'Structure of Materials under Extreme Conditions', Swiss-Norwegian Beamlines, European Synchrotron Radiation Facility, BP 220, F-38043 Grenoble cedex, France
[3] Laboratoire de Cristallographie, EPFL/SB/IPMC/LCR, École Polytechnique Fédéral de Lausanne, CH-1015 Lausanne, Switzerland
[4] Université du Maine-Cristallogenese, F-72025 Le Mans cedex, France

E-mail: andrzej@wm.lc.ehu.es

Abstract

The high-temperature behaviour of LiSrAlF$_6$ and LiCaAlF$_6$, both $P\bar{3}1c$ and $Z = 2$, was studied with high-resolution synchrotron angle-dispersive x-ray powder diffraction in the temperature ranges 150–823 and 298–723 K, respectively. No phase transitions were detected. The temperature dependencies of structural parameters and octahedral distortions are obtained with the Rietveld method. Both materials have highly anisotropic thermal expansion, with the c parameter in LiSrAlF$_6$ decreasing with increasing temperature. Our observations on the temperature evolution of various structural parameters, like interatomic distances, angles, distortions and polyhedral volumes indicate that the negative thermal expansion along the c axis in LiSrAlF$_6$ arises from concerted angular distortions around the Sr and Al atoms and diminished F$\cdots$F interatomic distances in the SrF$_6$ slabs. The SrF$_6$ slab contracts with increasing temperatures because of the diminishing F–Sr–F octahedral angles. The CaF$_6$ layer becoming thicker and relatively temperature insensitive angular distortions do not result in anomalous negative thermal expansion in LiCaAlF$_6$.

1. Introduction

Solid state lasers are usually based on oxide compounds containing rare earth elements [1]. The key property of a material to be useful as a laser-host is its high luminescence efficiency.

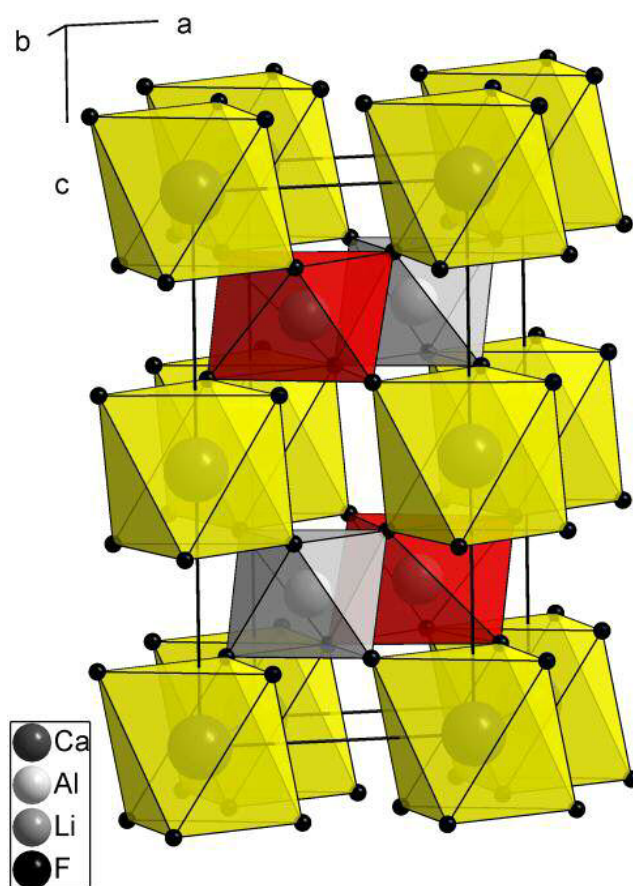[5] Author to whom any correspondence should be addressed.

Figure 1. Crystal structure of LiSrAlF$_6$ and LiCaAlF$_6$ at ambient conditions ($P\overline{3}1c$, $Z = 2$). (This figure is in colour only in the electronic version)

Fluorides are of interest as laser-host materials because of their large band gaps and low phonon energies resulting in lower multiphonon emission rates and high luminescence efficiencies when compared to oxides. Furthermore, they are stable with respect to radiation damage and they have small non-linear refractive indices [1, 2]. LiYF$_4$ is already a commercially used host material for laser systems. Several other rare-earth doped fluorides exhibit a luminescence output comparable to the LiYF$_4$ phosphor [3–6].

The *colquiriite* LiMM′F$_6$ (M = Ca or Sr; M′ = Al, Ga, or Cr) family of fluoride compounds is considered to be the most promising for optical applications [1–10]. The crystal structures of LiCaAlF$_6$ and LiSrAlF$_6$ ($P\overline{3}1c$, $Z = 2$) are ordered derivatives of the Li$_2$ZrF$_6$ type ($P\overline{3}1m$, $Z = 1$) [11]. Each cation occupies a deformed octahedral site (figure 1). The polyhedral distortions in LiMM′F$_6$ at ambient conditions have been correlated with the sizes of the M and M′ cations [9, 11, 12]. For the M site occupied by luminescent dopants, the distortion, larger for the Sr compounds, is associated with the relative rotations of the two opposite trigonal F faces. As a consequence, the strontium-containing materials provide larger optical absorption coefficients determined by the strengths of static and dynamic distortions of the crystal field [12].
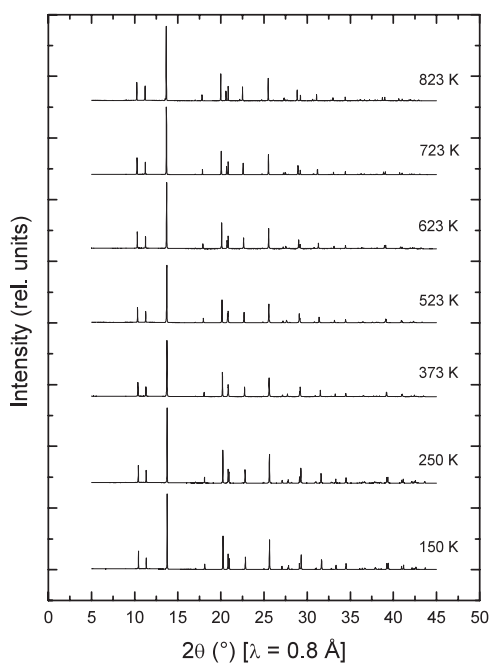
Figure 2. Selected x-ray powder diffraction patterns of LiSrAlF$_6$ at different temperatures in the 2θ region 5°–45°.

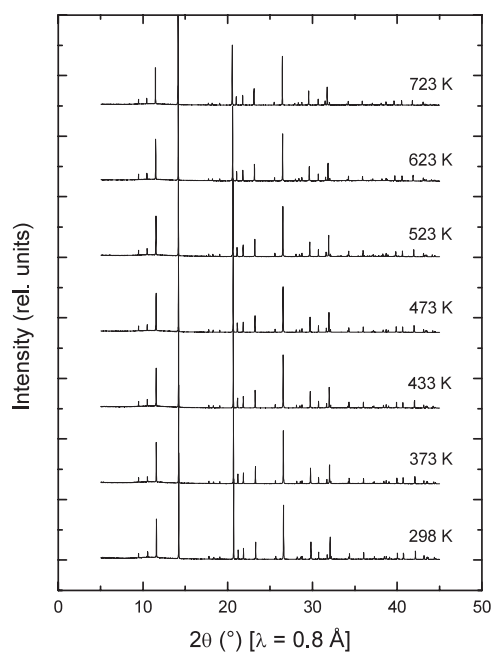**Figure 3.** X-ray powder diffraction patterns of LiCaAlF$_6$ at different temperatures in the 2θ region 5°–45°.

Figure 4. Observed, calculated and difference x-ray powder diffraction patterns for LiSrAlF$_6$ at 823 K as obtained after the final Rietveld refinement. Vertical markers indicate the positions of Bragg reflections. The inset shows the patterns in the 2θ range 35°–60° magnified five times.
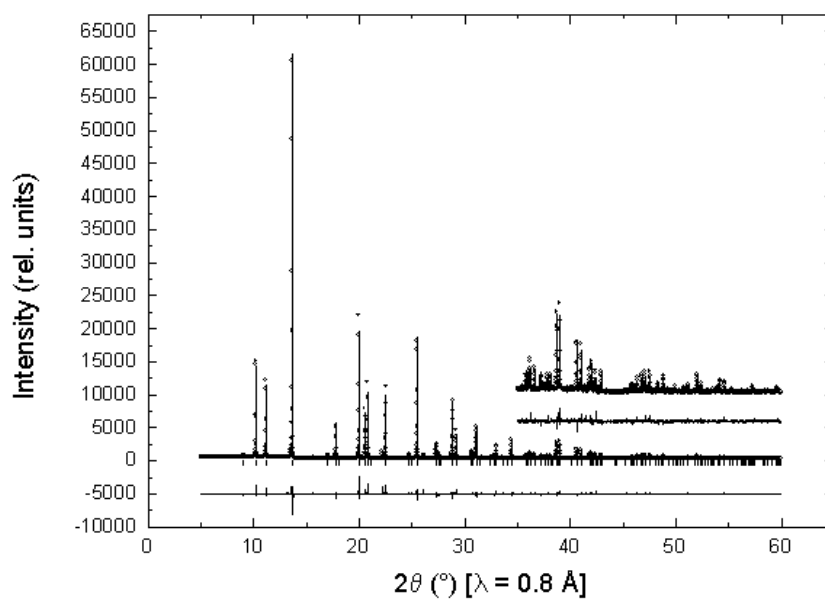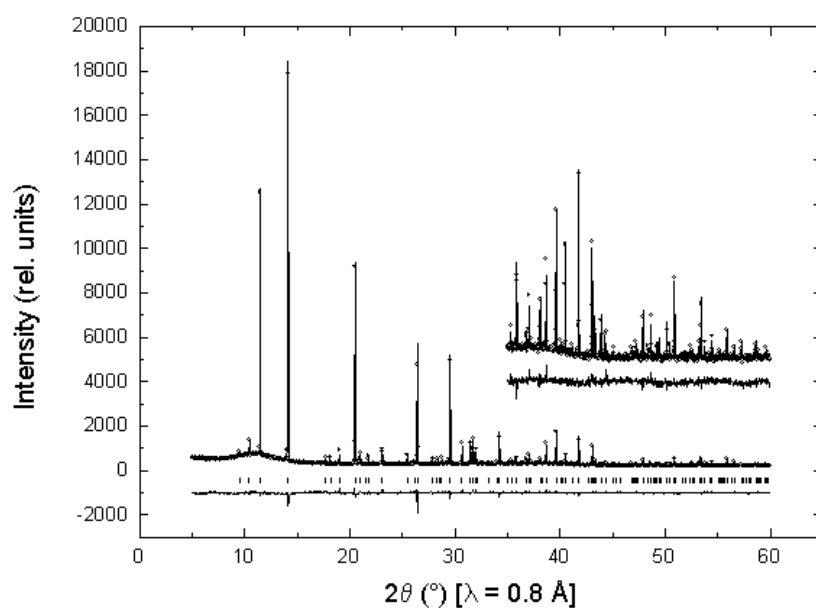
Figure 5. Observed, calculated and difference x-ray powder diffraction patterns for LiCaAlF$_6$ at 723 K as obtained after the final Rietveld refinement. Vertical markers indicate the positions of Bragg reflections. The inset shows the patterns in the 2θ range 35°–60° magnified five times.

Figure 6. Temperature dependence of lattice parameters and unit cell volumes in LiSrAlF$_6$ (open symbols) and LiCaAlF$_6$ (solid symbols). Representative estimated standard deviations are given in tables 1 and 2.

Figure 7. Temperature dependence of interatomic distances in LiSrAlF$_6$ (open symbols) and LiCaAlF$_6$ (solid symbols). Representative estimated standard deviations are given in tables 1 and 2.

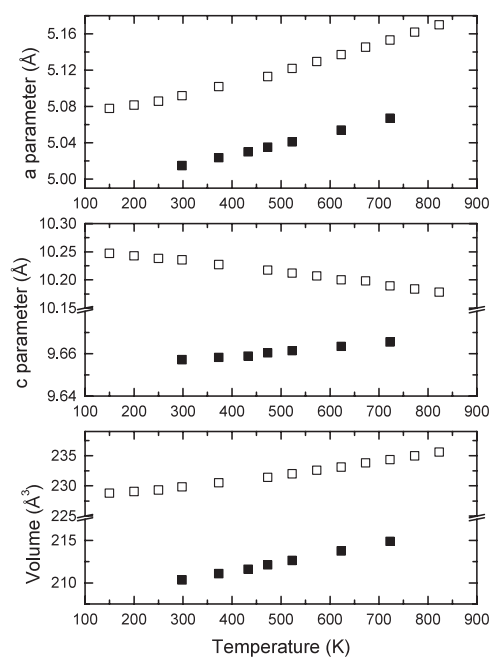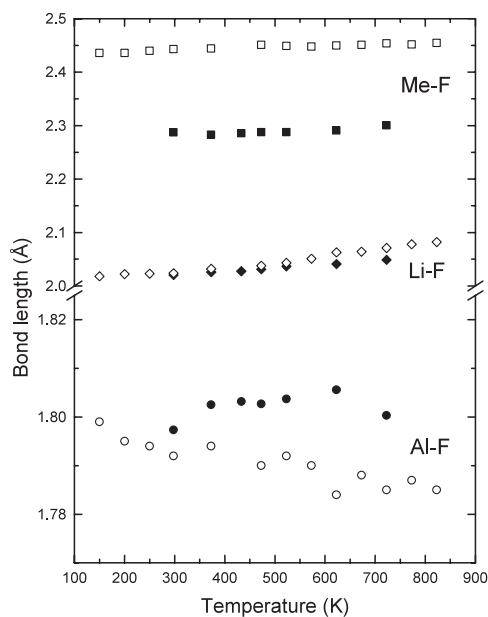**Table 1.** Structural parameters for LiSrAlF$_6$ ($P\bar{3}1c$, $Z = 2$) at 823 K, $a = 5.168\,79(2)$ Å, $c = 10.175\,51(6)$ Å. Estimated standard deviations are given in parentheses.

Atom	Site	x	y	z	U_i^*100
Li	2c	1/3	2/3	1/4	1.0
Sr	2b	0.0	0.0	0.0	3.90(3)
Al	2d	2/3	1/3	1/4	2.70(10)
F	12i	0.3934(4)	0.0430(5)	0.1489(2)	3.70(8)

Selected distances (Å)	
Li–F	2.082(2)
Sr–F	2.455(2)
Al–F	1.785(2)
F$\cdots$F	2.526(3)
	2.599(5)
	2.447(5)

Selected bond angles (deg)	
F–Li–F	97.69(9)
	71.98(12)
	94.30(12)
F–Sr–F	94.09(8)
F–Al–F	90.10(11)
	86.55(15)
	93.48(14)
Sr–F–Al	134.70(12)
Al–F–Li	100.73(11)
Sr–F–Li	119.37(8)

Preliminary studies of the temperature dependence of lattice parameters in LiCaAlF$_6$ and LiSrAlF$_6$ at the temperature range 298–600 K indicated that both materials have highly anisotropic thermal expansion, with the c parameter in LiSrAlF$_6$ decreasing with increasing temperature [12]. The anisotropic thermal expansion indicates a high sensitivity to thermal shocks and thermal gradients [10]. The thermal conductivity in these fluorides is smaller than the one in oxides and leads to higher temperature gradients during their crystal growth and laser action. The heat produced within the crystals during the application as laser hosts can thus lead to cracking.

This study aims to elucidate the structural origin of the anisotropic thermal expansion in *colquiriites* LiCaAlF$_6$ and LiSrAlF$_6$ by measuring their x-ray powder diffraction patterns as a function of temperature at ambient pressure. The temperature dependencies of structural parameters and octahedral distortions are obtained with the Rietveld method.

2. Experimental details

The polycrystalline samples of LiCaAlF$_6$ and LiSrAlF$_6$ studied here were the same as in previous reports on the high-pressure behaviour of the two compounds [13]. The x-ray powder patterns were measured in the Debye–Scherrer geometry (glass capillaries with the inner diameter of 0.3 mm) using a two-circle high-resolution multi-analyser diffractometer on the BM1B station at the ESRF (Grenoble, France) in the 2θ region 2°–60°. An intrinsic resolution was approximately 0.01° at a wavelength of 1 Å. The data were collected in the temperature

Table 2. Structural parameters for LiCaAlF$_6$ ($P\bar{3}1c$, $Z = 2$) at 723 K, $a = 5.065\,49(2)$ Å, $c = 9.663\,21(5)$ Å. Estimated standard deviations are given in parentheses.

Atom	Site	x	y	z	U_i^*100
Li	2c	1/3	2/3	1/4	1.0
Ca	2b	0.0	0.0	0.0	2.29(4)
Al	2d	2/3	1/3	1/4	2.12(7)
F	12i	0.3793(3)	0.0373(3)	0.1436(2)	2.99(5)

Selected distances (Å)	
Li–F	2.049(2)
Ca–F	2.300(2)
Al–F	1.800(1)
F$\cdots$F	2.560(2)
	2.571(3)
	2.493(3)

Selected bond angles (deg)	
F–Li–F	97.04(6)
	74.97(8)
	91.93(9)
F–Ca–F	92.64(6)
F–Al–F	90.64(7)
	87.66(10)
	91.14(11)
Ca–F–Al	135.00(8)
Al–F–Li	98.69(7)
Ca–F–Li	121.32(6)

Table 3. Linear thermal expansion coefficients in LiSrAlF$_6$ and LiCaAlF$_6$ ($\times 10^{-6}$ K^{-1}).

	LiSrAlF$_6$		LiCaAlF$_6$	
	α_{11}	α_{33}	α_{11}	α_{33}
This study	23.2(6)	−17.1(4)	20.4(3)	3.4(1)
[12] [a]	23.5	−6.6	22.9	2.5
[16]	18.8	−10.0		
[17]			22.0	3.6

[a] The units of $10^{-6}\,°C^{-1}$.

ranges 150–823 K for LiSrAlF$_6$ and 298–723 K for LiCaAlF$_6$ at atmospheric pressure. The wavelength was 0.8 Å.

Rietveld refinements of the diffraction patterns collected at different temperatures were carried out using the program GSAS [14]. The refined parameters included the lattice parameters, fractional atomic coordinates of the fluorine atoms, isotropic thermal parameters for the Me (Sr or Ca), Al and F atoms, Stephens profile function parameters [15], and overall intensity scaling factor. The isotropic thermal parameters for the Li atoms were fixed at an arbitrary value of 0.01 and not refined. This relatively low value was chosen to ensure a good localization of the light atom Li.
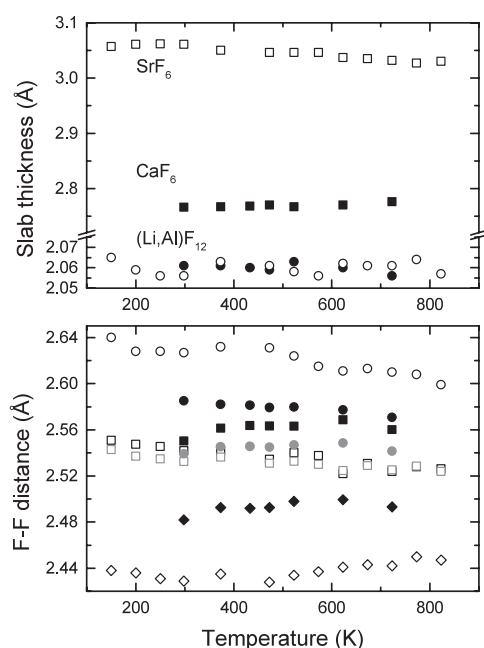
Figure 8. Temperature dependence of non-bonded F $\cdots$ F distances and of thicknesses of octahedral slabs along the c axis in LiSrAlF$_6$ (open symbols) and LiCaAlF$_6$ (solid symbols). The grey symbols stand for the average F $\cdots$ F distances. Representative estimated standard deviations for the non-bonded F $\cdots$ F distances are given in tables 1 and 2. The thicknesses were recalculated from the refined lattice and structural parameters with no estimated standard deviations.
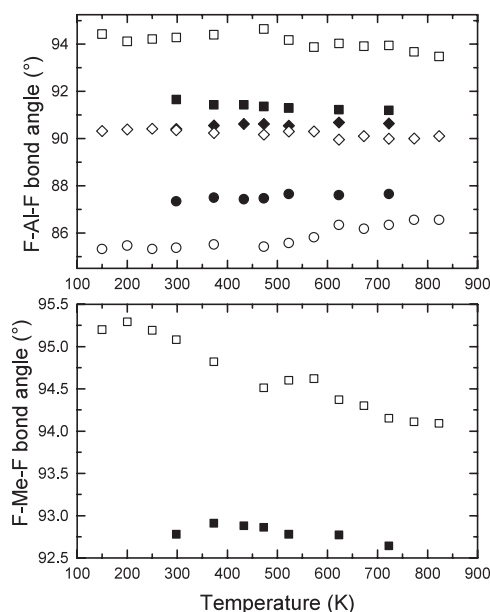
Figure 9. Temperature dependence of F–Al–F and F–Me–F angles in LiSrAlF$_6$ (open symbols) and LiCaAlF$_6$ (solid symbols). Representative estimated standard deviations are given in tables 1 and 2.

3. Results and discussion

X-ray powder patterns of LiSrAlF$_6$ and LiCaAlF$_6$ as a function of temperature are shown in figures 2 and 3, respectively. No phase transitions were observed in both compounds in the entire temperature ranges studied here. All the patterns of LiSrAlF$_6$ and LiCaAlF$_6$ were refined with the Rietveld method [14] using the structural models presented by Yin and Keszler [11] (tables 1 and 2, respectively). The best fit for LiSrAlF$_6$ at 823 K (table 1 and figure 4) was obtained with $R_{wp} = 10.88\%$, $R_p = 8.21\%$, $R(F^2) = 11.63\%$, and goodness of fit 2.11 (the residuals R_{wp} and R_p have been calculated with the background eliminated, see the GSAS manual [14]). The best fit for LiCaAlF$_6$ at 723 K (table 2 and figure 5) was obtained with $R_{wp} = 8.25\%$, $R_p = 6.88\%$, $R(F^2) = 16.23\%$, and goodness of fit 1.62 (the residuals R_{wp} and R_p have been calculated with the background eliminated; see the GSAS manual [14]).

The temperature dependence of lattice parameters and unit cell volumes in LiSrAlF$_6$ and LiCaAlF$_6$ is shown in figure 6. In accordance with previous reports [10, 12], the c lattice parameter in LiSrAlF$_6$ decreases upon heating. The linear thermal expansion coefficients α_{11} (along the a axis) and α_{33} (along the c axis) are defined as $(\mathrm{d}a/\mathrm{d}T)/a$ and $(\mathrm{d}c/\mathrm{d}T)/c$, respectively. The coefficients α_{11} and α_{33} in LiSrAlF$_6$ are 23.2×10^{-6} and $-17.1 \times 10^{-6}\,\mathrm{K}^{-1}$, respectively (table 3). The analogous parameters for LiCaAlF$_6$ are $\alpha_{11} = 20.4 \times 10^{-6}\,\mathrm{K}^{-1}$ and $\alpha_{33} = 3.4 \times 10^{-6}\,\mathrm{K}^{-1}$. They are compared with the values reported in [12, 16, 17] in table 3.
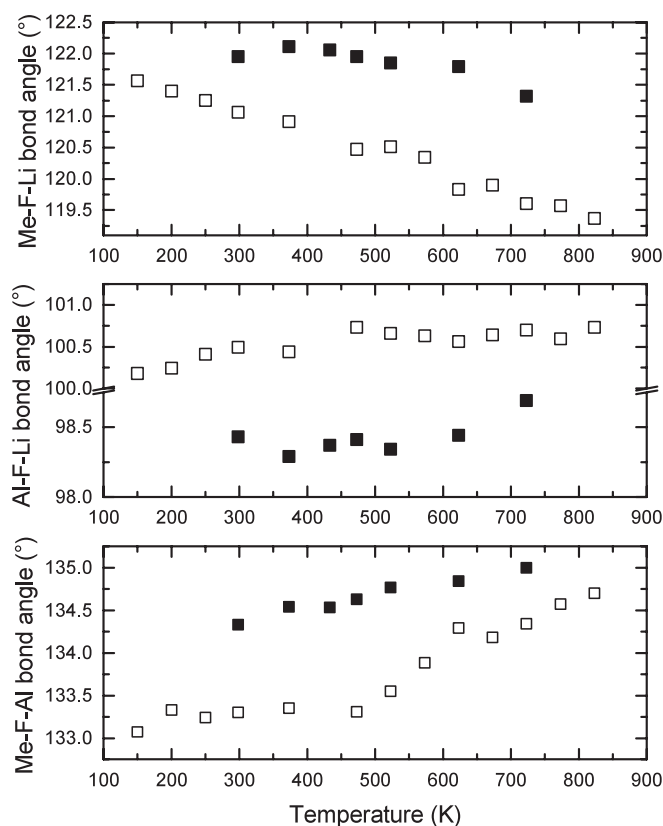
Figure 10. Temperature dependence of intra-octahedral angles in LiSrAlF$_6$ (open symbols) and LiCaAlF$_6$ (solid symbols). Representative estimated standard deviations are given in tables 1 and 2.

In the structures of LiCaAlF$_6$ and LiSrAlF$_6$, the adjacent LiF$_6$ and AlF$_6$ octahedra share edges and are connected to the CaF$_6$ and SrF$_6$ octahedra, respectively, by sharing the fluorine atoms at their vertices (figure 1). For the purpose of this study, these crystal structures are regarded as two-dimensional ones with an alternate stacking of (Li, Al)F$_{12}$ and CaF$_6$ or SrF$_6$ slabs along the c axis. The structural origin of negative thermal expansion along the c axis in LiSrAlF$_6$ can be elucidated by examining the temperature dependencies of interatomic distances, angles and distortions (figures 7–12). Figures 7 and 8 depict the evolution of the cation–fluorine bond lengths and non-bonded F$\cdots$F distances in both compounds. The striking features are the decreasing Al–F and the average F$\cdots$F distances in the strontium-containing compound. Such an evolution of the F$\cdots$F distances in LiSrAlF$_6$ is dominated by the shortening of the F–F octahedral edges around the Sr atoms, with the F$\cdots$F distance of 2.599 Å at 823 K (table 1). The thicknesses of the (Li, Al)F$_{12}$ slabs in both compounds do not change with increasing temperature and oscillate around the value of 2.06 Å (figure 8). Unlike the CaF$_6$ slabs in LiCaAlF$_6$, the SrF$_6$ layers in LiSrAlF$_6$ become thinner at high temperatures. Associated is a strong decrease both of the F–Sr–F (figure 9) and Sr–F–Li (figure 10) bond angles. The distortion from O$_h$ symmetry at the D$_3$ sites of the Al atoms could be measured by three angles (figure 9). The medium one, 90.11° in LiSrAlF$_6$ at 823 K (table 1) and 90.64° in LiCaAlF$_6$ at 723 K (table 2), corresponds to two F atoms in the same trigonal plane, while the
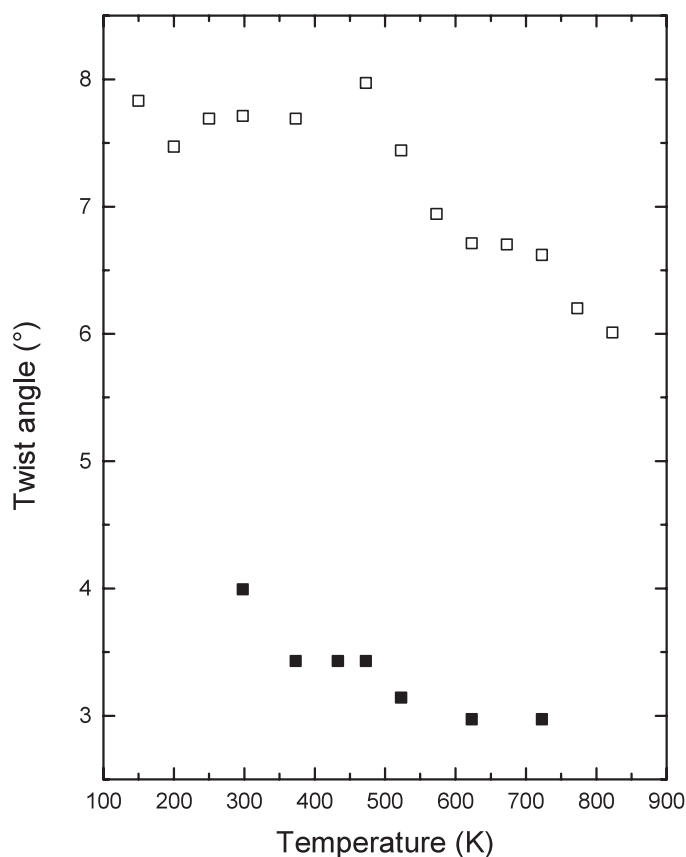
Figure 11. Temperature dependence of the MeF$_6$ twist angle in LiSrAlF$_6$ (open symbols) and LiCaAlF$_6$ (solid symbols). The angles were recalculated from the refined lattice and structural parameters with no estimated standard deviations.

other two correspond to interactions in opposite planes [11]. Unlike in LiCaAlF$_6$, the two large angles do not tend to merge in LiSrAlF$_6$ (figure 9). The deviations could also be measured by the relative orientations of the trigonal F planes perpendicular to the three-fold c axis. These planes are twisted from the ideal 60°. The twist angles in both compounds (figure 11) decrease with increasing temperatures. The Li atoms occupy highly distorted octahedral sites in both materials, with F–Li–F angles significantly deviating from ideal 90° [11]. These deviations increase at high temperatures (figure 12). The temperature evolution of octahedral volumes calculated using the program VOLCAL [18] is shown in figure 13. Except for the volume of the AlF$_6$ polyhedron in LiSrAlF$_6$, all the other polyhedral volumes have positive temperature dependencies.

Our observations on the temperature evolution of various structural parameters, like interatomic distances, angles, distortions and polyhedral volumes, indicate that the negative thermal expansion along the c axis in LiSrAlF$_6$ arises from concerted angular distortions around the Sr and Al atoms and shortened F$\cdots$F interatomic distances in the SrF$_6$ slabs. The SrF$_6$ slab contracts with increasing temperatures because of the diminishing F–Sr–F octahedral angles. At the same time, the thickness of the (Li, Al)F$_{12}$ layer in LiSrAlF$_6$, in which the AlF$_6$ octahedral volume diminishes upon heating, is approximately constant because the
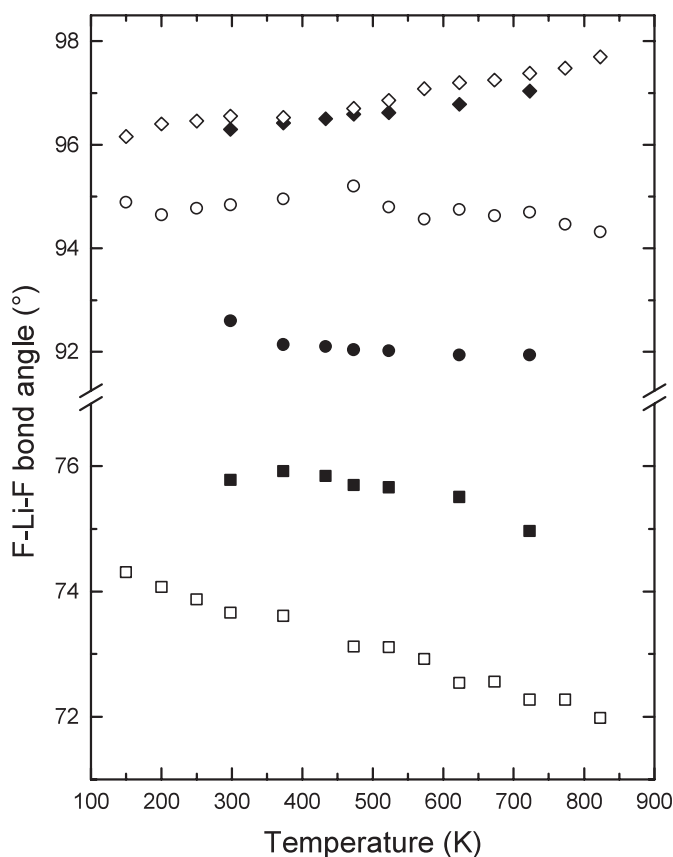
Figure 12. Temperature dependence of F–Li–F angles in $LiSrAlF_6$ (open symbols) and $LiCaAlF_6$ (solid symbols). Representative estimated standard deviations are given in tables 1 and 2.

interoctahedral angle Sr–F–Li significantly closes down. The CaF_6 layer becoming thicker and relatively temperature insensitive angular distortions in $LiCaAlF_6$ do not result in anomalous negative thermal expansion.

$LiSrAlF_6$ and $LiCaAlF_6$ have different behaviour not only at high temperatures and atmospheric conditions but also at high pressures and room temperature. The pressure-induced crystal structures of these two materials were previously studied with synchrotron angle-dispersive x-ray powder diffraction in a diamond anvil cell [13]. The structure of $LiSrAlF_6$-II ($P2_1/c$, $Z = 4$), stable between 1.6 and 3.0 GPa, is a distorted variant of the ambient pressure polymorph ($LiSrAlF_6$-I, $P\bar{3}1c$, $Z = 2$), in which each cation occupies a deformed octahedral site. $LiCaAlF_6$ transforms to this monoclinic polymorph II above about 7 GPa. $LiSrAlF_6$-III ($P2_1/c$, $Z = 4$), occurring above 3.0 GPa, is related to $LiBaCrF_6$ and built of deformed SrF_{12} icosahedra within a three-dimensional framework of corner-sharing distorted AlF_6 octahedra and LiF_4 tetrahedra. The pressure-induced changes of the coordination polyhedra in the series $LiSrAlF_6$-I, $LiSrAlF_6$-II to $LiSrAlF_6$-III are similar to the differences in coordination polyhedra due to the increase of the ionic radii of the Sr^{2+} and Ba^{2+} cations in $LiSrAlF_6$-I and $LiBaM''F_6$ ($M'' = Al$, Ga, Cr, V, Fe, or Ti) at ambient conditions.

The results of this study and the high-pressure investigations of $LiSrAlF_6$ and $LiCaAlF_6$ [13] suggest that the stability and thermal properties of these two materials depend
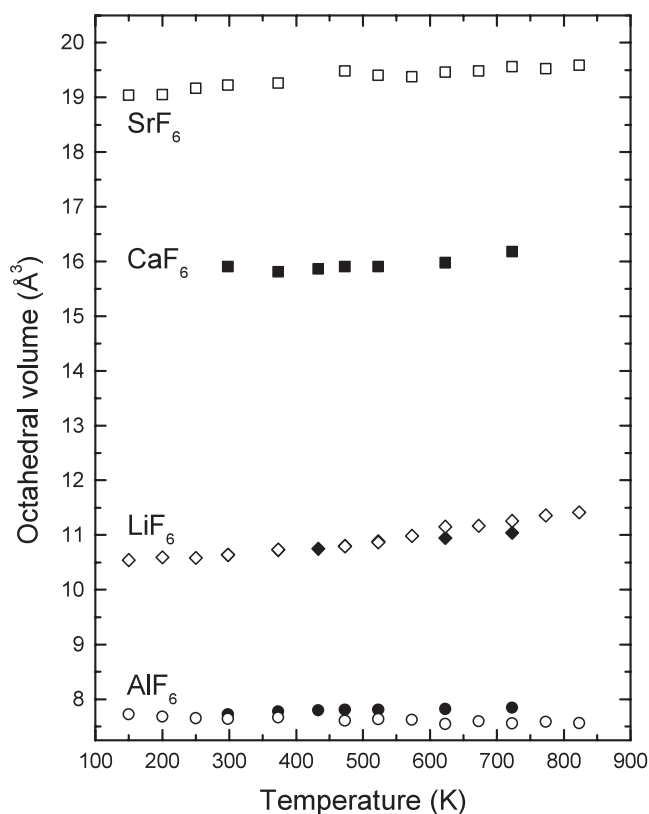
Figure 13. Temperature dependence of octahedral volumes in LiSrAlF$_6$ (open symbols) and LiCaAlF$_6$ (solid symbols). The data points for the LiF$_6$ octahedral volumes in both compounds partly overlap. The volumes were recalculated from the refined lattice and structural parameters with no estimated standard deviations.

on the alkaline-earth metal present, or, in general, on the radius of the cation at the 2b site (tables 1 and 2). Accordingly, an effect of a substitution of the Ca^{2+} cations for the Sr^{2+} ones in the solid solution series LiSr$_{1-x}$Ca$_x$AlF$_6$ to possibly obtain a material with no or nearly extinguished negative thermal expansion might as well be reproduced by introducing other divalent cations at this crystallographic site with radii smaller than the one for the Sr^{2+} ion.

Acknowledgments

References

[1] Burkhalter R, Dohnke I and Hulliger J 2001 *Prog. Cryst. Growth Charact.* **42** 1
[2] Joubert M F *et al* 2001 *J. Fluor. Chem.* **107** 235
[3] Sarantopoulou E, Kollia Z and Cefalas A C 2000 *Microelectron. Eng.* **53** 105
[4] Wells J P R *et al* 2000 *J. Lumin.* **87–89** 1029

        Tigreat P Y *et al* 2001 *J. Lumin.* **94/95** 23
 [5] Shimamura K *et al* 2002 *Opt. Mater.* **19** 109
 [6] Braud A *et al* 2000 *Phys. Rev.* B **61** 5280
        Braud A *et al* 2001 *Appl. Phys.* B **72** 909
 [7] Machado M A C *et al* 2002 *J. Phys.: Condens. Matter* **14** 271
 [8] Liu Z *et al* 2002 *Opt. Mater.* **19** 123
 [9] Ono Y *et al* 2001 *J. Cryst. Growth* **229** 505
        Pawlak D A *et al* 2001 *J. Cryst. Growth* **233** 699
[10] Klimm D and Reiche P 1999 *Cryst. Res. Technol.* **34** 145
        Sato H *et al* 2002 *Japan. J. Appl. Phys.* **41** 2028
[11] Yin Y and Keszler D A 1992 *Chem. Mater.* **4** 645
[12] Yamada M *et al* 1999 *J. Phys.: Condens. Matter* **11** 10499
        Martínez Vázquez R *et al* 2002 *J. Cryst. Growth* **237–239** 894
[13] Grzechnik A, Dmitriev V, Weber H-P, Gesland J-Y and van Smaalen S 2004 *J. Phys.: Condens. Matter*
        16 1033
        Grzechnik A, Dmitriev V, Weber H-P, Gesland J-Y and van Smaalen S 2004 *J. Phys.: Condens. Matter*
        16 3005
[14] Larson A C and von Dreele R B 2000 GSAS: general structure analysis system *Los Alamos National Laboratory*
        Report
[15] Stephens P W 1999 *J. Appl. Crystallogr.* **32** 281
[16] Smith L K, Payne S A, Tassano J B, DeLoach L D, Kway W L and Krupke W F 1993 *OSA Proc.* vol 15, p 381
[17] Woods B W, Payne S A, Marion J E, Hugues R S and Davis L E 1991 *J. Opt. Soc. Am.* B **8** 970
[18] Finger L W VOLCAL—program to calculate polyhedral volumes and distortion parameters
        http://www.ccp14.ac.uk/ccp/ccp14/ftp-mirror/larryfinger/VOLCAL.FOR